Is the ^{31}P Chemical Shift Anisotropy of Aluminophosphates a Useful Parameter for NMR Crystallography?

Daniel M. Dawson*, Robert F. Moran, Scott Sneddon and Sharon E. Ashbrook*

School of Chemistry, EaStCHEM and Centre of Magnetic Resonance, University of St Andrews, St Andrews KY16 9ST, United Kingdom

*Author to whom correspondence should be addressed.

Email: *sema@st-andrews.ac.uk*

dmd7@st-andrews.ac.uk

Submitted to *Magn. Reson. Chem. NMR Crystallography Special Edition.*

Abstract

The ^{31}P chemical shift anisotropy (CSA) offers a potential source of new information to help determine the structures of aluminophosphate framework materials (AlPOs). We investigate how to measure the CSAs, which are small (span of ~20-30 ppm) for AlPOs, demonstrating the need for CSA-amplification experiments (often in conjunction with ^{27}Al and/or ^{1}H decoupling) at high magnetic field (20.0 T) to obtain accurate values. We show that the most shielded component of the chemical shift tensor, δ_{33}, is related to the length of the shortest P-O bond, whereas the more deshielded components, δ_{11} and δ_{22} can be related more readily to the mean P-O bond lengths and P-O-Al angles. Using the case of Mg-doped STA-2 as an example, the CSA is shown to be much larger for $P(OAl)_{4-n}(OMg)_n$ environments, primarily owing to a much shorter P-O(Mg) bond affecting δ_{33}, however, since the mean P-O bond lengths and P-O-T (T = Al, Mg) bond angles do not change significantly between $P(OAl)_4$ and $P(OAl)_{4-n}(OMg)_n$ sites, the isotropic chemical shifts for these species are similar, leading to overlapped spectral lines. When the CSA information is included, spectral assignment becomes unambiguous, therefore, while the specialist conditions required might preclude the routine measurement of ^{31}P CSAs in AlPOs, in some cases (particularly doped materials), the experiments can still provide valuable additional information for spectral assignment.

Keywords: solid-state NMR spectroscopy, ^{31}P, chemical shift anisotropy, CSA, aluminophosphates, AlPOs, DFT calculations

Introduction

Aluminophosphates (AlPOs)[1] are a group of zeotypic materials, exhibiting porous structures that lead to a range of applications in gas storage and separation, drug delivery and catalysis.[2,3] AlPOs are conventionally synthesised hydrothermally (or solvothermally) in the presence of a cationic structure directing agent (SDA), resulting in open-pore structures. In pure aluminophosphate frameworks, the charge of the SDA is balanced by anions, *e.g.*, OH^- or F^-, that coordinate to the framework resulting in five- and six-coordinate Al species in addition to the expected four-coordinate, or tetrahedral, Al.[2,3] Calcination (typically at 500-600 °C) removes the SDA, charge-balancing anions and any water within the pores, resulting in a neutral $AlPO_4$ framework. It is also possible to balance the charge of the SDA (either completely or partially) through aliovalent substitution, *e.g.*, Mg^{2+}, Cr^{2+} or Zn^{2+} in place of Al^{3+} to give MeAPOs, or Si^{4+} in place of P^{5+} in SAPOs (where, in the calcined MeAPOs or SAPOs, the anionic framework charge is balanced by Brønsted acid sites), giving the framework catalytic and/or redox properties.[2-5]

The structural characterisation of AlPOs is frequently based on Bragg diffraction data, typically from powder or single-crystal X-ray diffraction (XRD). However, while the unit cell parameters and/or coordinates of the framework atoms can usually be determined reasonable accurately, extraframework species within the pores frequently exhibit either static or dynamic disorder.[6-10] Furthermore, the charge-balancing anions do not necessarily respect the symmetry and order of the framework itself.[11-13] Therefore, any crystal structures obtained for such materials describe a spatially and temporally averaged structure that may not be representative of the local chemical environment of any one atom at any given time.

Nuclear magnetic resonance (NMR) spectroscopy can provide valuable chemical and structural information for solids, owing to the sensitivity of the NMR parameters to variations in the local (*i.e.*, atomic-scale) geometry.[14-17] This approach does not require

any long-range order and is sensitive to dynamics on timescales over several orders of magnitude, providing an ideal complement to diffraction-based methods, especially for the study of disordered materials. For AlPOs in particular, the presence of many NMR-active nuclei in the framework, the SDA and the charge-balancing anions enables detailed information on all aspects of the local structure to be extracted.[5,16,17] The isotropic chemical shift is able to provide information on the number and type of coordinating atoms, as well as next-nearest neighbours, while information on covalent bonding or spatial proximities can be obtained through experiments that transfer magnetisation *via* the J coupling or dipolar coupling, respectively.[15] However, these interactions are anisotropic, resulting in broad and often featureless spectral lineshapes for powdered solids.

It is now relatively routine to carry out density functional theory (DFT) calculations in order to help interpret the complex spectral lineshapes that are often observed in solid-state NMR spectra.[18-22] In particular, periodic DFT codes using the Gauge-Including Projector Augmented Wave (GIPAW) approach have enabled the accurate calculation of NMR parameters in solids.[18,21,23] Such calculations have been applied to AlPOs; enabling spectral assignment,[8,24,25] improving understanding of the relationship between structure and NMR parameters,[26] and providing insight into the disorder (both positional and temporal) of the SDAs, water, charge-balancing anions and framework substitutions.[7,8,11,27,28] A pre-requisite for the calculation or prediction of NMR parameters is a structural model, although for disordered materials these are often adapted and modified from ordered structures of similar materials, with a number of possible structures considered. It is often necessary to optimise the geometry to an energy minimum in order to obtain good agreement with experimental NMR spectra.[7,21,29] The use of semi-empirical dispersion-correction (SEDC) schemes has been demonstrated to have a significant impact on the longer-range structures obtained after DFT optimisation for calcined and as-prepared AlPOs, with structures optimised using SEDC schemes having better agreement between calculated and experimental NMR and XRD parameters.[29,30]

To provide high-resolution isotropic NMR spectra of solids, techniques such as magic angle spinning (MAS) or decoupling are frequently employed.[14,15] These methods do, however, discard much of the anisotropic information, which may still be of use in understanding the structure of the materials. In principle, the chemical shift anisotropy (CSA) can provide structural information directly (*e.g.*, in recent work in pyrochlore ceramics the ^{89}Y CSA was shown to be directly correlated with the Y-O bond length[31]), or by comparison to predictions using DFT calculations for a variety of structural models. The ability to consider more than one NMR parameter when refining or choosing between models can also improve confidence in the result and ease the understanding and interpretation of NMR spectra. For a powdered sample, the principal components of the chemical shift tensor can be determined from static or (more usually) slow MAS experiments. In the latter case, the sideband manifold reflects the static lineshape and the tensor components can be obtained from an analytical fit.[32] However, for samples with more than one distinct species, overlap of sidebands and centrebands from different sites can hamper the extraction of accurate information. Furthermore, when very slow MAS is required to obtain a sufficient number of sidebands (*i.e.*, for very small anisotropies), dipolar interactions may not be efficiently removed, hindering the spectral resolution. An alternative approach is to use experiments that reintroduce the CSA in the indirect dimension of a pseudo two-dimensional experiment, producing an individual sideband manifold that can be analysed for each site, while enabling the use of fast MAS to provide high-resolution spectra. Furthermore, the CSA can be "amplified", resulting in an apparently slower MAS rate in the indirect dimension, producing more sidebands and enabling the accurate measurement of smaller CSAs in fast MAS experiments.[33-36] Although a number of approaches for these measurements exist, this work uses the CSA-amplified PASS experiment,[35,36] which has previously been shown to be robust for the measurement of ^{1}H, ^{13}C, ^{31}P, ^{89}Y and ^{119}Sn CSAs in a range of organic and inorganic materials.[31,35-37]

Here, we investigate the relationship between structure and ^{31}P CSA in microporous aluminophosphate frameworks. We explore whether the CSA can be measured accurately, and also investigate the use of periodic DFT to calculate CSA parameters, and the methods that are required to ensure accurate results are obtained. Finally, we consider if, and how, the interaction parameters can be directly related to the local geometry. We primarily focus on pure aluminophosphate frameworks (in both as-prepared and calcined forms), but also consider the application of the experimental and theoretical approaches we use to the study of disordered (Mg-doped) AlPOs and evaluate their use as potential tools for future structure solution of more complex phosphate-based frameworks.

Methods

Synthesis

The synthesis of the AlPOs studied here (see Table 1) has been described previously in the literature, along with the basic characterisation of the samples.[7,24,25,28,29,49] All calcined AlPOs were dried in an oven at ~110 °C for 24 h directly prior to the acquisition of NMR spectra.

Solid-state NMR spectroscopy

Solid-state NMR spectra were acquired using Bruker Avance III spectrometers, equipped with 14.1 and 20.0 T wide-bore superconducting magnets, and operating at ^{31}P Larmor frequencies of 242.94 and 344.14 MHz, respectively. Samples were packed in conventional 4 mm rotors and rotated at MAS rates of up to 14 kHz. Chemical shifts are shown in ppm relative to 85% H_3PO_4, using BPO_4 (δ_{iso} = –29.6 ppm[14]) as a secondary reference. Where necessary, to improve spectral resolution, continuous wave (CW) or SPINAL-64 ^{1}H decoupling was applied during acquisition, with a typical radiofrequency field strength, ν_1, of ~100 kHz. For as-prepared and calcined AlPO-14, low-power CW ^{27}Al decoupling was also employed (ν_1 of ~10 kHz), as this has previously been shown to be essential to

enable resolution of all four resonances present.[50] Spectra were acquired using a recycle interval of 30 s for as-prepared AlPOs and 5 s for calcined AlPOs.

Two-dimensional CSA-amplified PASS experiments used the pulse sequence of Orr *et al.* (see the Supporting Information).[35,36] The total scaling factor is given by $N_T = (n_{PASS} + 1)N$, where N is the scaling factor determined by the timings of the five π pulses and n_{PASS} is the number of additional π pulse blocks used. Cogwheel phase cycling was employed to reduce the length of the phase cycle required,[51,52] and decoupling (either of ^{1}H and/or ^{27}Al) was applied during acquisition. Further details are given in the Supporting Information. Fitting of the sideband manifolds extracted from the two-dimensional spectra was carried out using SIMPSON[53,54] by comparison to a conventional MAS spectrum simulated at the apparent MAS rate. The root-mean-square (rms) errors quoted are output by SIMPSON, as defined in the SIMPSON manual. Using the Herzfeld-Berger convention,[55] with the principal components of the shift tensor, δ, ordered such that $\delta_{11} \geq \delta_{22} \geq \delta_{33}$, the isotropic chemical shift, δ_{iso}, is given by $\delta_{iso} = (\delta_{11} + \delta_{22} + \delta_{33})/3$, the magnitude of the anisotropy (span) $\Omega = \delta_{11} - \delta_{33}$, and the skew, $\kappa = 3(\delta_{22} - \delta_{iso})/\Omega$ (such that $-1 \leq \kappa \leq 1$).

DFT calculations

Calculations of NMR parameters were carried out using the CASTEP DFT code (version 5.5.2),[56] employing the gauge-including projector augmented wave (GIPAW) approach,[23] to reconstruct the all-electron wavefunction in the presence of a magnetic field. Calculations were carried out using the GGA PBE functional[57] and core-valence interactions were described by ultrasoft pseudopotentials.[58] A planewave energy cutoff of 50 Ry (~680 eV) was used, and integrals over the Brillouin zone used a Monkhorst-Pack grid with a k-point spacing of 0.04 2π Å^{-1}. Initial atomic positions and unit cell parameters for all structures were taken from the literature (see Table 1). For structural optimisations, the SEDC scheme of Tkatchenko and Scheffler,[59] as implemented by McNellis *et al.*[60] was used to include dispersion interactions. Calculations were carried out at the University of St Andrews using a 300-node (3600-core) Intel Westmere cluster with 2 GB memory per

core and QDR Infiniband interconnects. Calculations generate the absolute shielding tensor ($\boldsymbol{\sigma}$) in the crystal frame, and diagonalisation of the symmetric part yields the three principal components σ_{11}, σ_{22} and σ_{33}. From these, $\sigma_{iso}^{calc} = (\sigma_{11} + \sigma_{22} + \sigma_{33})/3$, $\Omega^{calc} = \sigma_{11} - \sigma_{33}$ and $\kappa^{calc} = 3(\sigma_{22} - \sigma_{iso})/\Omega^{calc}$.

Geometry-based calculations

Structural parameters (bond lengths and angles) were obtained using either DISCO 17.11[61] or in-house Python scripts based on the MagResPython library.[62] Structure-spectrum relationships were determined using MATLAB[63] routines as described elsewhere.[61]

Results and Discussion

Measurement of CSAs in Pure AlPOs

The tetrahedral PO_4 environments found in AlPOs might be expected to yield small CSAs owing to their high symmetry. This is most likely to be the case for the neutral and purely tetrahedral framework of calcined AlPOs, whereas the extraframework ions in as-prepared materials, or framework cation substitution (in MeAPOs and SAPOs), may well result in a greater anisotropy. The structures of many AlPOs have more than one crystallographically-distinct P site, and it is not always possible to choose a MAS rate that is sufficiently slow to obtain the requisite number of sidebands for CSA determination,[64] but also avoids the coincidental overlap of isotropic resonances and spinning sidebands. This can be seen in Figure 1a, where ^{31}P MAS NMR spectra of as-prepared AlPO-14, show that the resonances from the four distinct P sites (two very closely spaced, with $\delta_{iso} = -5.4$, –19.6, –20.3, and −24.1 ppm, for P2, P4, P1 and P3, respectively[24]) can be resolved at 14 kHz MAS (with ^{27}Al CW decoupling), but 1.75 kHz MAS results not only in a complex spectrum with considerable signal overlap, but also in significant broadening of the spectral lineshapes, as a result of the inefficient averaging of the dipolar interactions. This reduced resolution prevents accurate site-specific analysis of the sideband manifolds. Figure 1b shows a ^{31}P two-dimensional CSA-amplified PASS spectrum of as-prepared

AlPO-14, acquired using N_T = 7, resulting in an apparent MAS rate of 2 kHz in the indirect dimension. This results in between 8 and 11 spinning sidebands for each resonance, as shown in Figure 1c, but retains the high-resolution associated with fast MAS in the direct dimension. Low-power CW ^{27}Al decoupling was used in acquisition in order to resolve the P4 and P1 resonances. High-power ^{1}H decoupling was used in spectral acquisition for all as-prepared AlPOs, as shown in the Supporting Information. Values of Ω and κ extracted from the sideband manifolds for each of the four P sites (as shown in Figures 1c and 1d), are given in Table 2, along with those for four other as-prepared AlPOs: AlPO-15, JDF-2, AlPO-34 and SIZ-4. The relatively low rms errors (< 6 for most P sites) confirm the accuracy of the values extracted. For JDF-2, a much higher rms error (~35) is observed for one resonance. However, this results from the overlap of signals from P1 and P3, complicating the sideband analysis. It was not possible to resolve these two resonances, even using ^{27}Al and ^{1}H decoupling. Figure 2a shows that the range of Ω for ^{31}P in as-prepared AlPOs (~50 ppm) is larger than that of δ_{iso} (~20 ppm), perhaps suggesting it could prove a more sensitive probe of structural differences and changes in AlPOs. The magnitude of Ω is relatively low in all cases (25-70 ppm), reflecting the tetrahedral nature of the PO_4 environment. It can also be seen from Figure 2a that there is no correlation between δ_{iso} and Ω for these materials.

It might be expected that the PO_4 environments of calcined AlPOs would be even more symmetrical than in as-prepared AlPOs, leading to smaller ^{31}P CSAs. Such small CSAs would necessitate the use of very large scaling factors in CSA-amplified PASS experiments, which requires higher values of n_{PASS} (see the Supporting Information). In previous work,[35,36] scaling factors of up to 27 were used, but were accompanied by a loss of signal (up to 50% for the highest values used). Furthermore, if decoupling is applied throughout the sequence, care must be taken to ensure that the duty cycle remains low enough to prevent any probe damage. Table 3 shows the values of ^{31}P δ_{iso}, Ω and κ for calcined AlPO-14, AlPO-17, AlPO-18, AlPO-34 and AlPO-53(B), extracted from two-dimensional CSA-amplified PASS spectra. In all cases, N_T of 10.67 was used, resulting in an effective MAS rate in the indirect dimension of 1.312 kHz. For AlPO-14, low power CW

^{27}Al decoupling was also applied to resolve the distinct P species. The rms errors are relatively low, suggesting accurate results are obtained. For AlPO-18, three crystallographically-distinct P sites are present in the proposed crystal structure, but only one resonance was observed experimentally, even when ^{27}Al and ^{1}H decoupling were used, as observed previously.[29] As a result, the sideband manifold is expected to result from the combination of the three different signals. (See below for further discussion). Figure 2b shows that smaller ranges of both δ_{iso} and Ω are present for the calcined AlPOs, reflecting the greater similarity in the local environments present. Once again, the spread of Ω (~20 ppm) is greater than that of δ_{iso} (~10 ppm). Despite the greater variation in Ω than δ_{iso}, the greater challenge associated with measuring the smaller CSAs results more experimental uncertainty and, perhaps, less discrimination between materials.

Although the interactions that affect NMR spectra encode information on the local structure, the exact relationship between geometrical and spectroscopic parameters can be complex, hindering real structure "solution" from a single spectrum. Conversely, the sensitivity of the NMR parameters to small changes in structure could enable different structural models or proposals to be validated or refined, if the NMR parameters could be accurately predicted and compared to experiment. Recent work[20,21,24,29,30] has shown that periodic DFT calculations can successfully predict ^{31}P and ^{27}Al NMR parameters for AlPOs (following appropriate optimisation, as discussed in detail by Sneddon *et al*.[29]). In this work, crystal structures were taken from the literature (see Table 1) and optimised as described above. NMR parameters were calculated for structures before and after optimisation (see the Supporting Information for more details). Calculated values are given in Tables 4 and 5. Note that for AlPO-18, where the structural model from diffraction predicts three crystallographically-distinct P sites, the calculated isotropic shifts are very similar, in agreement with the experimental observation of a single resonance, as noted earlier. The extraction of a single Ω from the experimental spectrum, is also supported by the similarity of the three values of Ω^{calc}.

Figures 3a and 3b show plots of Ω^{calc} against Ω^{exp} for the as-prepared and calcined AlPOs both prior to ($\Omega^{calc,unopt}$) and post ($\Omega^{calc,opt}$) optimisation. For the as-prepared AlPOs, agreement between calculation and experiment is poor prior to optimisation but significantly better for the optimised structures, although the points show some scatter around an ideal 1 : 1 correlation. For calcined AlPOs (Figures 3c and 3d), much greater spread in Ω^{calc} is observed for the non-optimised structures, with significant deviation from the 1 : 1 correlation. However, for optimised structures the agreement with experiment is much better, although, as discussed above, there is relatively little spread in the values. Any disagreement between calculation and experiment in this case is likely to be due not only to the inaccuracy of the computational approach, but also to the uncertainties in the experimental measurements. Figure 3 shows the sensitivity of Ω to small changes in the local structure and its potential use in NMR crystallography for structure refinement of as-prepared AlPOs but suggests that, for calcined AlPOs, measurement will not be generally useful, except in the cases of more extreme structures.

To assess whether the accuracy of the experimental measurements affects the quality of the agreement between experiment and calculation for calcined AlPOs, CSA-amplified PASS NMR spectra were also recorded at higher field (20.0 T), where the magnitude of the CSA (in Hz) is increased. Consequently, the number of spinning sidebands observed increases, potentially improving the accuracy of the fit. The experimental parameters used are given in the Supporting Information. Figure 4a plots $\Omega^{calc,opt}$ against Ω^{exp} for the data acquired at 20.0 T (see also the Supporting Information). The high-field data agree slightly better with the calculated values, with a larger number of points lying closer to the 1 : 1 correlation. Figure 4b compares Ω^{exp} for the experiments recorded at the two separate fields. Although the two measurements appear to be in reasonable agreement, there is a general trend towards overestimation of Ω^{exp} at lower field. However, the 20.0 T data confirm that the CSAs for calcined AlPOs are both very small and very similar, perhaps suggesting that there may be little to be gained from its measurement for many (although clearly not all) calcined AlPOs.

Relationships between the CSA and Local Structure

As early as the 1980s, spectroscopists were seeking empirical relationships between ^{31}P NMR spectra of phosphates and their crystal structures.[14] However, many of these studies concern phosphate salts (containing isolated Q^0 rather than connected Q^4 PO_4 tetrahedra as found in AlPOs), are subject to relatively large experimental uncertainties (particularly in the crystal structures), or are only applicable to a small set of structurally related materials. More recently, we demonstrated that, for ^{31}P in both calcined[26] and as-prepared[61] AlPOs, and the similar case of ^{29}Si in silica zeolites,[65] δ_{iso} depends on a combination of both the mean P-O (or Si-O) bond length and the mean P-O-Al (or Si-O-Si) bond angle, suggesting that the CSA may also be predicted from these structural parameters. As in the previous work, to investigate this here we relate the calculated NMR parameters to the DFT-optimised structures to avoid the introduction of experimental errors. Figure 5 shows that there is no clear dependence of ^{31}P $\Omega^{calc,opt}$ on the mean P-O bond length, $\langle r_{PO} \rangle$, or P-O-Al bond angle, $\langle \theta_{POAl} \rangle$. This is perhaps to be expected, given that, unlike the isotropic chemical shift (*i.e.*, an average value) the CSA has an orientation dependence and may, therefore, be expected to depend more strongly on the individual bond lengths and angles than on their average values. The deviation of the PO_4 geometry from tetrahedral can be described by various parameters, including the distortion index, DI, and the longitudinal strain, $|\alpha|$. The DI is a measure of the deviation from ideality of the O-P-O bond angles, θ_{OPO}, within a PO_4 tetrahedron, and is given by

$$\mathrm{DI} = \sum_{i=1}^{n} \frac{\left|\theta_{OPO(0)} - \theta_{OPO(i)}\right|}{n} \quad , \qquad (1)$$

where the ideal bond angle, $\theta_{OPO(0)}$, is 109.47° and n = 6 for a tetrahedron. The longitudinal strain is a measure of the deviation from the ideal bond length, $r_{PO(0)}$, (defined as the bond length of an ideal tetrahedron of the same volume as the distorted tetrahedron in question), given by

$$|\alpha| = \sum_{i=1}^{n} \left| \ln\left(\frac{r_{PO(i)}}{r_{PO(0)}} \right) \right| \quad , \qquad (2)$$

where the individual P-O bond lengths are ordered with $r_{PO(1)} \leq r_{PO(2)} \leq r_{PO(3)} \leq r_{PO(4)}$. It is not possible to define a deviation from an "ideal" P-O-Al bond angle, as this value will be

dictated by the longer-range topology of the AlPO in question. For the as-prepared AlPOs (Figure 5a), there is little correlation between $\Omega^{calc,opt}$ and either the DI or $|\alpha|$, even though these parameters describe a deviation from the expected isotropic value. A similar situation is observed for the calcined AlPOs, as shown in Figure 5b, although the situation is exacerbated here by the much smaller distributions of the bond lengths and angles: a reflection of the more idealised PO_4 tetrahedra observed in the optimised structures of calcined AlPOs.[29] Nevertheless, it is clear that the CSA must be dependent on the structure as, in favourable cases (*e.g.*, axial symmetry), the shape (if not the width) of the powder-pattern lineshape can be readily predicted. Grimmer *et al*.[66] attempted to relate the ^{29}Si CSA in silicates to the lengths of the individual Si-O bonds, arguing that the most shielded component of the magnetic shielding tensor (σ_{33}) should be aligned with the shortest Si-O bond (where the electron density will be closest to the Si atom),[67] albeit on a small set of materials with axial or cubic symmetry at the Si site. This argument is intuitive and, as can be seen from Figure 6a, appears to hold at least partially for the AlPOs studied here, where σ_{11} and σ_{22} do not appear to be correlated with the shortest P-O bond length, whereas σ_{33} shows a moderate correlation, with $R^2 = 0.49$. As can be seen from Figures 6b-d, σ_{33} is not correlated with the other three P-O bond lengths at all, whereas σ_{11} and σ_{22} have higher correlation coefficients (R^2 ~0.4 to ~0.8, see Table 6 for values) for these bond lengths. As shown in Figure 6e, both σ_{11} and σ_{22} show an even stronger correlation with $\langle r_{PO} \rangle$, which is not surprising given their dependence on three of the four contributions to this term. However, σ_{33}, which appears to be influenced by only one of the four bond lengths ($r_{PO(1)}$), is effectively independent of $\langle r_{PO} \rangle$. Plots of σ_{ii} against the individual P-O-Al bond angles (see Figure S4.1 of the Supporting Information) show that σ_{33} is also effectively independent of the P-O-Al bond angle, whereas σ_{11} and σ_{22} depend more strongly on all bond angles (R^2 of ~0.4 to ~0.9).

Using a similar multivariate linear regression approach to our previous work[27,62] on AlPOs (see the Supporting Information for more details), it was possible to derive terms relating the principal components of $\boldsymbol{\sigma}$ to the local structure, with

$$\sigma_{11} = -1493 + 2558\langle r_{PO} \rangle - 952.7\langle r_{PO} \rangle^2 - 701.0\sigma(r_{PO})$$

$$- 126.9\cos(\langle\theta_{POAl}\rangle) + 0.3778\sigma(\theta_{POAl}) \ , \quad (3)$$

$$\sigma_{22} = -2118 + 1473\langle r_{PO}\rangle - 467.2\,\sigma(r_{PO}) - 214.3\cos(\langle\theta_{POAl}\rangle) - 0.1537\sigma(\theta_{POAl}) \ , \quad (4)$$

and

$$\sigma_{33} \sim 2129 - 1189 r_{PO(1)} - 210.3\sigma(r_{PO}), \quad (5)$$

where $\sigma(r_{PO})$ and $\sigma(\theta_{POAl})$ are the standard deviations in r_{PO} and θ_{POAl}, respectively. As can be seen from Figure 7, these expressions provide reasonably good predictions of σ_{11} and σ_{22}, but the prediction of σ_{33} is poor. It is interesting to note that the average of the three predicted σ_{ii}, corresponding to σ_{iso} and given by

$$\sigma_{iso} = -494.1 - 396.2\, r_{PO(1)} + 1344\langle r_{PO}\rangle - 317.6\langle r_{PO}\rangle^2 - 459.5\sigma(r_{PO}) - 113.7\cos(\langle\theta_{POAl}\rangle) + 0.07467\sigma(\theta_{POAl}), \quad (6)$$

does not, at first sight, agree particularly well with that from Ref. [61]. As discussed in the Supporting Information, its predictive power is quite similar, although the increased coefficient for $\sigma(r_{PO})$ is likely a consequence of the relatively small distribution of P-O bond lengths in the optimised structures considered here and is likely to lead to greater errors when predicting σ_{iso} for more distorted AlPO structures.

^{31}P CSAs in Doped AlPOs

As shown above, the ^{31}P CSA can be related to the local structure in AlPOs but, owing to the relatively small magnitude of this value, experimental measurement is challenging and, perhaps, not of significant practical benefit. However, this drawback arises from the fact that the PO_4 tetrahedra in AlPOs are generally highly symmetric and the anisotropy may be expected to be larger in less symmetric structures. This was demonstrated by Phillippou *et al.*,[68] who used magic angle turning (MAT) experiments to measure the ^{31}P CSA for $P(OAl)_{4-n}(OMg)_n$ sites in Mg-doped AlPO-20 (SOD-type framework with a single P site in the pure $AlPO_4$ form). For the symmetric $P(OAl)_4$ site, it was not possible to measure the CSA tensor (at 9.4 T), which is perhaps to be expected given the above discussion. However, for the $P(OAl)_3(OMg)_1$ site, a large span (74.3 ppm) was observed and the κ of 0.63 reflects the "pseudo-C_3" symmetry (*i.e.*, close to axial, $\kappa = \pm 1$) of the environment. For $P(OAl)_2(OMg)_2$, the span was similar (78.0 ppm) whereas the κ of 0.24 was indicative of "pseudo-C_{2v}" symmetry (*i.e.*, κ is closer to 0 in the absence of a high-

symmetry rotation axis). The $P(OAl)_1(OMg)_3$ did not have a lineshape characteristic of a well-defined CSA, perhaps owing to the lower intensity of this resonance. Here, we attempt to explore the information available from ^{31}P CSAs of doped AlPOs using the example of Mg-doped STA-2. STA-2 has the SAT framework and was first prepared as a Mg-doped material.[69,70] Subsequently, it was prepared in the pure AlPO form,[28] and Seymour *et al*.[11] have since carried out a detailed investigation of the disorder of the charge-balancing OH^- anions in this form. At a Mg : Al : P ratio of 1 : 5 : 6, no extraframework anions are required for charge balancing and any disorder arises from the distribution of Mg within the framework. Seymour *et al*.[27] used a combination of solid-state NMR spectroscopy, DFT calculations and powder XRD measurements to show that Mg^{2+} preferentially substitutes onto the Al1 site, but full assignment of the ^{31}P NMR spectrum was not possible owing to an extensive overlap of the spectral resonances.

Figure 8 shows the ^{31}P MAS NMR spectra of AlPO-STA-2 and Mg-doped STA-2 with a Mg : Al : P ratio of 1 : 5 : 6, overlaid with the CSA measured by CSA-amplified PASS experiments at regular intervals across the lineshapes. For both materials, the range of isotropic chemical shifts is from –15 to –32 ppm (the broad resonances between 0 and –15 ppm correspond to amorphous phosphate impurities that are common in the synthesis of AlPOs). However, the CSA measurements reveal greater differences between the two materials, with the pure AlPO form exhibiting small spans (typically below 50 ppm) across the entire lineshape, whereas the resonances between –15 and –21.5 ppm in the Mg-doped material have Ω between 65 and 80 ppm, confirming their assignment as $P(OAl)_3(OMg)$ and $P(OAl)_2(OMg)_2$ species, in agreement with the assignment of Seymour *et al.* on the basis of calculated isotropic chemical shifts.

The results shown in Figure 8 suggest that additionally measuring the ^{31}P CSA for doped AlPOs can provide greater insight into the spectral assignment than the isotropic shifts alone, which must often be compared to computational results from limited structural models in order to arrive at a tentative assignment. Indeed, in the case of Mg-doped STA-2, spectral assignment is easier on the basis of only the experimental CSAs

than isotropic shifts, even when compared to calculation, although clearly the latter are more easily determined experimentally. In a series of calculations carried out on 66 structural models of Mg-doped STA-2 (see the Supporting Information for further details), the P-O bonds in P-O(Mg) linkages were observed to be 1.501(7) Å, which is significantly shorter than the 1.536(11) Å observed for the P-O bonds in P-O(Al) linkages. However, the mean P-O bond lengths change very little between $P(OAl)_4$, $P(OAl)_3(OMg)$ and $P(OAl)_2(OMg)_2$ sites, with a slight (~0.3 pm) increase per next-nearest neighbour Mg cation, owing to the tendency for the P-O(Al) bonds to lengthen to compensate for the shorter P-O(Mg) bonds (thereby maintaining the total bond valence for P) – see the Supporting Information for more details. There are also small differences (on average, ~3°) in the P-O-Al and P-O-Mg bond angles (see the Supporting Information), although these are more constrained by the overall framework topology. The similar $\langle r_{PO} \rangle$ and $\langle \theta_{POT} \rangle$ for $P(OAl)_{4-n}(OMg)_n$ with n = 0 to 2 would be expected to lead to similar isotropic chemical shifts (as observed experimentally). However, as discussed above, the magnitude of the CSA is at least partially dependent on the shortest P-O bond length (owing to the dependence of σ_{33}, but not σ_{11}, on this parameter), and the increased span for the $P(OAl)_{4-n}(OMg)_n$ (n = 1, 2) sites can be explained relatively readily, at least qualitatively.

Attempts either to use Equations 3-5 to predict ^{31}P σ_{ii} from the local structure for MgAPO STA-2, or to reparameterise the equations using the MgAPO STA-2 data as input were insufficiently accurate to be of practical use. This failure prevents the immediate inclusion of CSA predictions in DISCO,[61] where such information could be of benefit, *e.g.*, for relating molecular dynamics simulations of reactions catalysed by doped phosphate frameworks to experimental measurements. However, there is a clear (and presumably general) structural rationale for the increased span observed for $P(OAl)_{4-n}(OMg)_n$ sites, meaning that the measurement of ^{31}P CSAs in doped phosphates will still be of great benefit when attempting to interpret the complex spectra often observed for these disordered materials.

Conclusions

The ^{31}P chemical shift anisotropy (CSA) of aluminophosphates has been shown to be difficult to measure accurately, even using CSA-amplified PASS experiments and high (20.0 T) magnetic field. This is due in most part to the small span of the chemical shift tensor, arising from the highly symmetric PO_4 tetrahedra present, especially in calcined AlPOs. Although the possible presence of ^{31}P homonuclear dipolar interactions could affect the accuracy of experimental measurements at lower MAS rates, faster sample spinning, particularly at higher magnetic fields necessitates the use of very high scaling factors in the amplified PASS experiment, which can lead to lineshape distortions and inaccurate results.[31]

The most shielded component of the magnetic shielding tensor, σ_{33}, is related to the length of the shortest P-O bond, whereas the more deshielded components, σ_{11} and σ_{22} are related more readily to the mean P-O bond lengths and P-O-Al bond angles. The average of the three predicted σ_{ii} values also yields a good prediction of the isotropic shielding, σ_{iso}, with a mean absolute error of 1.2 ppm. However, owing to the experimental error in measuring the principal components of the chemical shift tensor for AlPOs (particularly once calcined), this information is unlikely to be of significant practical benefit unless there is an extremely short P-O bond present owing to some unusual framework distortions.

In contrast to the pure aluminophosphates, Mg-doped AlPOs exhibit much larger ^{31}P CSAs for $P(OAl)_{4-n}(OMg)_n$ environments, arising predominantly from short P-O bonds in P-O-Mg linkages, which affect only one component of the shielding tensor. However, the overall mean P-O bond lengths and P-O-T (T = Al, Mg) bond angles do not change greatly between $P(OAl)_4$ and $P(OAl)_{4-n}(OMg)_n$ sites meaning that the isotropic chemical shifts for these species are similar and complex overlapped resonances are observed in the MAS spectrum. However, the inclusion of the CSA measurement leads to an unambiguous spectral assignment. Despite the clear qualitative relationship between structure and the spectrum for MgAPO-STA-2, quantitative prediction of σ_{ii} from the structural models was unsuccessful, perhaps owing to some further structural parameters that have not been considered here.

While the specialist conditions required are likely to preclude the routine measurement of ^{31}P CSAs in AlPOs, we have demonstrated that in certain cases the experiments may still be worthwhile and provide valuable additional information for spectral assignment and interpretation.

Acknowledgements

We are grateful to EPSRC for support through the Collaborative Computational Project on NMR Crystallography (CCP-NC), *via* EP/M022501/1, and for a studentship to SS. SEA would also like to thank the Royal Society and Wolfson Foundation for a merit award. This research made use of the EaStCHEM Research Computing Facility. The UK 850 MHz solid-state NMR Facility used in this research was funded by EPSRC and BBSRC (contract reference PR140003), as well as the University of Warwick including via part funding through Birmingham Science City Advanced Materials Projects 1 and 2 supported by Advantage West Midlands (AWM) and the European Regional Development Fund (ERDF). Collaborative assistance from the 850 MHz Facility Manager (Dinu Iuga, University of Warwick) is acknowledged. The research data (and/or materials) supporting this publication can be accessed at DOI: 10.17630/ba570d0a-59a1-43d6-8d1a-c2ff2ef1f2f9.

References

[1] S. T. Wilson, B. M. Lok, C. A. Messina, T. R. Cannan, E. M. Flanigen, *J. Am. Chem. Soc.* **1982**, *104*, 1446.

[2] P. A. Wright, *Microporous Framework Solids*, RSC Publishing, Cambridge, **2008**.

[3] J. Yu, R. Xu, *Chem. Soc. Rev.* **2006**, *35*, 593.

[4] H. O. Pastore, S. Coluccia, L. Marchese, *Annu. Rev. Mater. Res.* **2005**, *35*, 351.

[5] H. Nagashima, C. Martineau-Corcos, G. Tricot, J. Trebosc, F. Pourpoint, J.-P. Amoureux, O. Lafon., *Ann. Rep. NMR Spectrsoc.* **2018**, 94, 113-185.

[6] S. Antonijevic, S. E. Ashbrook, S. Biedasek, R. I. Walton, S. Wimperis, H. Yang, *J. Am. Chem. Soc.* **2006**, *128*, 8054.

[7] S. E. Ashbrook, M. Cutajar, J. M. Griffin, Z. A. D. Lethbridge, R. I. Walton, S. Wimperis, *J. Phys. Chem. C* **2009**, *113*, 10780.

[8] D. M. Dawson, J. M. Griffin, V. R. Seymour, P. S. Wheatley, S. E. Ashbrook, M. Amri, R. I. Walton, N. Guillou, T. Kurkiewicz, S. Wimperis, *J. Phys. Chem. C* **2017**, *121*, 1781.

[9] A. Tuel, J.-L. Jorda, V. Gramlich, C. Baerlocher, *J. Solid State Chem.*, **2005**, *178*, 782.

[10] G. Poulet, P. Sautet, A. Tuel, *J. Phys. Chem. B*, **2002**, *106*, 8599.

[11] V. R. Seymour, E. C. V. Eschenroeder, M. Castro, P. A. Wright, S. E. Ashbrook, *CrystEngComm* **2013**, *15*, 8668.

[12] C. Martineau, B. Bouchevreau, Z. Tian, S.-J. Lohmeier, P. Behrens, F. Taulelle, *Chem. Mater.* **2011**, *23*, 4799.

[13] C. Martineau, C. Mellot-Draznieks, F. Taulelle, *Phys. Chem. Chem. Phys.* **2011**, *13*, 18078.

[14] K. J. D. MacKenzie, M. E. Smith, *Multinuclear Solid-State NMR of Inorganic Materials* Pergamon Press, Oxford, **2002**.

[15] S. E. Ashbrook, D. M. Dawson, J. M. Griffin, *Solid-State NMR Spectroscopy* in: *Local Structural Characterisation*, D.W. Bruce, D. O'Hare, R.I. Walton (Eds.), John Wiley & Sons Ltd, Chichester, **2014**.

[16] S. E. Ashbrook, D. M. Dawson, V. R. Seymour, *Phys. Chem. Chem. Phys.* **2014**, *16*, 8223.

[17] R. F. Moran, D. M. Dawson, S. E. Ashbrook, *Int. Rev. Phys. Chem.* **2017**, *36*, 39.

[18] C. Bonhomme, C. Gervais, F. Babonneau, C. Coelho, F. Pourpoint, T. Azais, S. E. Ashbrook, J. M. Griffin, J. R. Yates, F. Mauri, C. J. Pickard, *Chem. Rev.* **2012**, *112*, 5733.

[19] T. Charpentier, *Solid State Nucl. Magn. Reson.* **2011**, *40*, 1.

[20] S. E. Ashbrook, D. M. Dawson, *Acc. Chem. Res.* **2013**, *46*, 1964.

[21] S. E. Ashbrook, D. M. McKay, *Chem. Commun.* **2016**, *52*, 7186.

[22] *NMR Crystallography*, Ed. R. K. Harris, R. E. Wasylishen, M. J. Duer, John Wiley & Sons, **2009**.

[23] C. J. Pickard, F. Mauri, *Phys. Rev. B* **2001**, *63*, 245101.

[24] S. E. Ashbrook, M. Cutajar, C. J. Pickard, R. I. Walton, S. Wimperis, *Phys. Chem. Chem. Phys.* **2008**, *10*, 5754.

[25] P. J. Byrne, J. E. Warren, R. E. Morris, S. E. Ashbrook, *Solid State Sci.*, **2009**, *11*, 1001.

[26] D. M. Dawson, S. E. Ashbrook, *J. Phys. Chem. C* **2014**, *118*, 23285.

[27] V. R. Seymour, E. C. V. Eschenroeder, P. A. Wright, S. E. Ashbrook, *Solid State Nucl. Magn. Reson.* **2014**, *65*, 64.

[28] M. Castro, V. R. Seymour, D. Carnevale, J. M. Griffin, S. E. Ashbrook, P. A. Wright, D. C. Apperley, J. E. Parker, S. P. Thompson, A. Fecant, N. Bats, *J. Phys. Chem. C* **2010**, *114*, 12698.

[29] S. Sneddon, D. M. Dawson, C. J. Pickard, S. E. Ashbrook, *Phys. Chem. Chem. Phys.* **2014**, *16*, 2660.

[30] F. Vasconcelos, S. Cristol, J.-F. Paul, L. Montagne, F. Mauri, L. Delevoye, *Magn. Reson. Chem.* **2010**, *48*, S142.

[31] M. R. Mitchell, D. Carnevale, R. Orr, K. R. Whittle, S. E. Ashbrook, *J. Phys. Chem. C* **2012**, *116*, 4273.

[32] U. Haeberlen, *Advances in Magnetic Resonance*, Academic Press, New York, **1976**.

[33] O. N. Antzutkin, *Prog. Nucl. Magn. Reson. Spectrosc.* **1999**, *35*, 203.

[34] L. Shao, J. J. Titman, *Prog. Nucl. Magn. Reson. Spectrosc.* **2007**, *51*, 103.

[35] R. M. Orr, M. J. Duer, S. E. Ashbrook, *J. Magn. Reson.* **2005**, *174*, 301.

[36] R. M. Orr, M. J. Duer, *Solid State Nucl. Magn. Reson.* **2006**, *30*, 1.

[37] A. Fernandes, D. McKay, S. Sneddon, D. M. Dawson, S. Lawson, R. Veazey, K. R. Whittle, S. E. Ashbrook, *J. Phys. Chem. C* **2016**, *120*, 20288.

[38] C. Baerlocher; L. B. McCusker. *Database of Zeolite Structures*: http://www.iza-structure.org/databases/

[39] R. W. Broach, S. T. Wilson, R. M. Kirchner, *Micropor. Mesopor. Mater.* **2003**, *57*, 211.

[40] E. Aubert, F. Porcher, M. Souhassou, C. Lecomte, *Acta. Cryst.* **2003**, *B59*, 687.

[41] M. M. Harding, B. M. Kariuki, *Acta. Cryst.* **1994**, *C50*, 852.

[42] A. M. Chippindale, A. V. Powell, R. H. Jones, J. M. Thomas, A. K. Cheetham, Q. Huo, R. Xu, *Acta. Cryst.* **1994**, *C50*, 1537.

[43] E. R. Parnham, R. E. Morris, *Chem. Mater.* **2006**, *18*, 4882.

[44] R. W. Broach, S. T. Wilson, R. M. Kirchner, in *Proceedings of the 12th International Zeolite Conference*, ed. M. M. J. Treacy, B. C. Marcus, M. E. Bisher, J. B. Higgins, Materials Research Society, Warrendale, **1999**, vol. 3, p. 1715.

[45] M. P. Attfield, A. W. Sleight, *Chem. Mater.* **1998**, *10*, 2013.

[46] A. Simmen, L. B. McCusker, C. Baerlocher, W. M. Meier, *Zeolites* **1991**, *11*, 654.

[47] M. Amri, R. I. Walton, *Chem. Mater.* **2009**, *21*, 3380.

[48] R. M. Kirchner, R. W. Grosse-Kunstleve, J. J. Pluth, S. T. Wilson, R. W. Broach, J. V. Smith, *Micropor. Mesopor. Mater.* **2003**, *39*, 319.

[49] J. M. Griffin, L. Clark, V. R. Seymour, D. W. Aldous, D. M. Dawson, D. Iuga, R. E. Morris, S. E. Ashbrook, *Chem. Sci.* **2012**, *3*, 2293.

[50] L. Delevoye, C. Fernandez, C. M. Morais, J.-P. Amoureux, V. Montouillout, J. Rocha, *Solid State Nucl. Magn. Reson.* **2002**, *22*, 501.

[51] M. H. Levitt, P. K. Madhu, C. E. Hughes, *J. Magn. Reson.* **2002**, *155*, 300.

[52] N. Ivchenko, C. E. Hughes, M. H. Levitt, *J. Magn. Reson.* **2003**, *164*, 286.

[53] M. Bak, J. T. Rasmussen, N. C. Nielsen, *J. Magn. Reson.* **2000**, *147*, 296.

[54] http://nmr.au.dk/software/simpson/

[55] J. Herzfeld, A. E. Berger, *J. Chem. Phys.* **1980**, *73*, 6021.

[56] M. D. Segall, P. J. D. Lindan, M. J. Probert, C. J. Pickard, P. J. Hasnip, S. J. Clark, M. C. Payne, *J. Phys.* **2002**, *14*, 2717.

[57] J. P. Perdew, K. Burke, M. Ernzerhof, *Phys. Rev. Lett.* **1996**, *77*, 3865.

[58] J. R. Yates, C. J. Pickard, F. Mauri, *Phys. Rev. B* **2007**, *76*, 024401.

[59] A. Tkatchenko, M. Scheffler, *Phys. Rev. Lett.* **2009**, *102*, 073005.

[60] E. R. McNellis, J. Meyer, K. Reuter, *Phys. Rev. B* **2009**, *80*, 205414.

[61] D. M. Dawson, V. R. Seymour, S. E. Ashbrook, *J. Phys. Chem. C* **2017**, *121*, 28065.

[62] S. Sturniolo, T. F. G. Green, R. M. Hanson, M. Zilka, K. Refson, P. Hodgkinson, S. P. Brown, J. R. Yates, *Solid State Nucl. Magn. Reson.* **2016**, *78*, 64.

[63] MATLAB and Statistics Toolbox Release 2011b, The MathWorks, Inc., Natick, MA.

[64] P. Hodgkinson, L. Emsley, *J. Chem. Phys.* **1997**, *107*, 4808.

[65] D. M. Dawson, R. F. Moran, S. E. Ashbrook, *J. Phys. Chem. C* **2017**, *121*, 15198.

[66] A. R. Grimmer, *Chem. Phys. Lett.* **1985**, *119*, 416.

[67] A. R. Grimmer, R. Peter, E. Fechner, G. Molgedey, *Chem. Phys. Lett.* **1981**, *77*, 331.

[68] A. Philippou, F. Salehirad, D.-P. Luigi, M. W. Anderson, *J. Phys. Chem. B* **1998**, *102*, 8974.

[69] G. W. Noble, P. A. Wright, P. Lightfoot, R. E. Morris, K. J. Hudson, A. Kvick, H. Graafsma, *Angew. Chem. Int. Ed. Engl.* **1997**, *36*, 81.

[70] G. W. Noble, P. A. Wright, A. Kvick, *J. Chem. Soc. Dalton Trans.* **1997**, 4485.

Table 1. Details of the AlPOs used in this work.

Material	Framework type[38]	Extraframework species	Structure ref.
AlPO-14	AFN	isopropylammonium hydroxide, water	[39]
AlPO-15	-[a]	ammonium hydroxide	[40]
AlPO-34	CHA	morpholinium fluoride	[41]
JDF-2	AEN	methylammonium hydroxide	[42]
SIZ-4	CHA	1,3-dimethylimidazolium fluoride	[43]
calcined AlPO-14	AFN	-	[44]
calcined AlPO-17	ERI	-	[45]
calcined AlPO-18	AEI	-	[46]
calcined AlPO-34	CHA	-	[47]
AlPO-53(B)	AEN	-	[48]
MgAPO STA-2	SAT	1,4-bis-*N*-quinuclidiniumbutane	[28]

[a] AlPO-15 has not been assigned an IZA framework type code.

[b] Ref. [45] incorrectly states $a = b = 13.89787(7)$ Å, which should be $a = b = 13.089787(7)$ Å. This was corrected prior to all calculations.

Table 2. Experimental (14.1 T) ^{31}P NMR parameters (δ_{iso}, Ω and κ) and rms errors for as-prepared AlPOs.

	δ_{iso} (ppm)	Ω (ppm)	κ	rms error
AlPO-14				
P1	−20.3(1)	63.4(35)	0.3(1)	3.0
P2	−5.4(1)	40.0(21)	0.1(1)	2.5
P3	−24.1(1)	44.0(28)	0.3(1)	3.6
P4	−19.6(1)	59.8(36)	0.3(1)	3.1
AlPO-15				
P1	−11.9(1)	43.8(24)	0.2(2)	1.4
P2	−18.2(1)	37.1(10)	0.0(3)	0.7
JDF-2				
P1 + P3	−24.9(2)	28.1(36)	1.0(1)	35.5
P2	−13.4(1)	41.1(43)	0.0(1)	6.8
AlPO-34[a]				
P1	−7.6(1)	58.1(44)	0.1(1)	4.3
P2	−29.8(1)	60.2(51)	0.2(1)	4.5
P3	−23.8(1)	49.0(27)	0.1(1)	4.6
SIZ-4[a]				
P1	−7.6(1)	73.1(37)	0.1(1)	2.4
P2	−28.5(1)	67.4(35)	0.3(1)	2.6
P3	−22.5(1)	46.8(30)	0.2(1)	4.3

[a] Note that, for consistency and ease of comparison of data, the P sites in the isostructural AlPO-34 and SIZ-4 are numbered according to the scheme of Dawson *et al.*[8]

Table 3. Experimental (14.1 T) ^{31}P NMR parameters (δ_{iso}, Ω and κ) and rms errors for calcined AlPOs.

	δ_{iso} (ppm)	Ω (ppm)	κ	rms error
AlPO-14				
P1	−21.3(1)	38.4(34)	0.1(1)	4.6
P2	−27.1(1)	26.1(14)	0.0(1)	2.0
P3	−31.3(1)	20.6(13)	0.0(1)	0.7
P4	−26.1(1)	25.8(14)	0.0(1)	2.0
AlPO-53B				
P1	−29.9(1)	29.3(15)	0.0(2)	1.6
P2	−31.5(1)	24.6(16)	0.0(1)	0.4
P3	−26.8(1)	27.6(15)	0.0(2)	0.4
AlPO-34				
P1	−30.1(1)	27.3(14)	0.0(2)	3.9
AlPO-17				
P1	−26.1(1)	30.4(16)	0.0(1)	11.7
P2	−37.1(1)	30.1(16)	0.1(1)	5.2
AlPO-18				
P1 + P2 + P3	−27.6(1)	28.5(15)	0.0(1)	4.3

Table 4. Calculated ^{31}P NMR parameters ($\sigma_{iso}^{calc,opt}$, $\Omega^{calc,opt}$ and $\kappa^{calc,opt}$) for as-prepared AlPOs.

	$\sigma_{iso}^{calc,opt}$ (ppm)	$\Omega^{calc,opt}$ (ppm)	$\kappa^{calc,opt}$
AlPO-14			
P1	298.4	70.7	−0.4
P2	281.1	41.5	−0.4
P3	300.8	55.3	−0.4
P4	296.4	64.9	−0.5
AlPO-15			
P1	289.1	33.6	−0.6
P2	295.8	28.0	−0.5
JDF-2			
P1	302.3	38.1	−0.2
P2	288.5	43.7	0.4
P3	302.1	40.8	−0.3
AlPO-34[a]			
P1	283.5	51.1	−0.4
P2	310.3	68.2	−0.4
P3	302.2	56.2	−0.1
SIZ-4[a]			
P1	283.1	79.4	−0.3
P2	307.2	63.6	−0.7
P3	299.7	46.6	−0.7

[a] Note that, for consistency and ease of comparison of data, the P sites in the isostructural AlPO-34 and SIZ-4 are numbered according to the scheme of Dawson *et al.*[8]

Table 5. Calculated ^{31}P NMR parameters ($\sigma_{iso}^{calc,opt}$, $\Omega^{calc,opt}$ and $\kappa^{calc,opt}$) for calcined AlPOs.

	$\sigma_{iso}^{calc,opt}$ (ppm)	$\Omega^{calc,opt}$ (ppm)	$\kappa^{calc,opt}$
AlPO-14			
P1	299.7	39.8	−0.4
P2	306.2	23.6	−0.2
P3	312.3	12.1	0.4
P4	305.1	24.4	0.2
AlPO-53B			
P1	310.2	12.2	0.1
P2	311.8	26.6	0.3
P3	306.0	20.5	−0.1
AlPO-34			
P1	310.2	24.2	−0.1
AlPO-17			
P1	308.6	22.5	0.2
P2	315.7	17.8	−0.6
AlPO-18			
P1	309.4	22.7	−0.2
P2	309.8	22.9	0.0
P3	309.6	23.5	0.0

Table 6. Values of R^2 for the plots of $\sigma_{ii}^{calc,opt}$ against $r_{PO(i)}$ and $\langle r_{PO} \rangle$, shown in Figure 6.

	R^2 for $\sigma_{11}^{calc,opt}$	R^2 for $\sigma_{22}^{calc,opt}$	R^2 for $\sigma_{33}^{calc,opt}$
$r_{PO(1)}$	0.0003	0.0025	0.4982
$r_{PO(2)}$	0.2477	0.4104	0.0011
$r_{PO(3)}$	0.6774	0.7169	0.0093
$r_{PO(4)}$	0.7703	0.6268	0.0058
$\langle r_{PO} \rangle$	0.8530	0.8274	0.0665

Figure captions

Figure 1. (a) ^{31}P (14.1 T) NMR spectra of as-prepared AlPO-14, acquired at MAS rates of 14.0 and 1.75 kHz (with CW decoupling of ^{1}H in both cases and ^{27}Al CW decoupling at 14 kHz MAS). (b) ^{31}P (14.1 T, 14 kHz MAS) two-dimensional CSA-amplified PASS spectrum of as-prepared AlPO-14, with $N_T = 7$ giving an apparent MAS rate of 2 kHz in F_1. For other experimental details, see the Supporting Information. (c) Extracted (normalised) spinning sideband manifolds (black) and analytical fits (red), and (d) contour plots of the rms error (arbitrarily truncated at 25) for each of the four P sites.

Figure 2. Plots of experimental ^{31}P span (Ω) against isotropic shift (δ_{iso}) for each P site in (a) as-prepared and (b) calcined AlPOs.

Figure 3. Plots of calculated span ($\Omega^{calc,unopt}$ and $\Omega^{calc,opt}$) against experimental span (Ω^{exp}) for each P site in (a, b) as-prepared and (c, d) calcined AlPOs. Calculations were carried out (a, c) before and (b, d) after geometry optimisation. The broken grey lines indicate a 1 : 1 correlation.

Figure 4. Plots of (a) ^{31}P $\Omega^{calc,opt}$ against Ω^{exp} measured at 20.0 T and (b) Ω^{exp} measured at 20.0 T against Ω^{exp} measured at 14.1 T for calcined AlPOs. The broken grey lines indicate a 1 : 1 correspondence.

Figure 5. Plots showing the variation in ^{31}P $\Omega^{calc,opt}$ with changes in the mean P-O bond distance, $\langle r_{PO} \rangle$, mean P-O-Al bond angle, $\langle \theta_{POAl} \rangle$, distortion index, DI, and longitudinal strain, $|\alpha|$, for (a) as-prepared and (b) calcined AlPOs.

Figure 6. Plots of $\sigma_{ii}^{calc,opt}$ against (a-d) the individual P-O bond lengths, $r_{PO(i)}$ and (e) $\langle r_{PO} \rangle$ for each P site in all as-prepared and calcined AlPOs. The components σ_{ii} are ordered with $\sigma_{33} \geq \sigma_{22} \geq \sigma_{11}$ and the bond lengths are ordered with $r_{PO(1)} \leq r_{PO(2)} \leq r_{PO(3)} \leq r_{PO(4)}$. The lines

of best fit are indicated for each plot, with the values of R^2 for each of these lines given in Table 6.

Figure 7. Plots of predicted σ_{ii} and σ_{iso} (from Equations 3-6) against the values calculated by DFT ($\sigma_{ii}^{calc,opt}$ and $\sigma_{iso}^{calc,opt}$) for all as-prepared and calcined AlPOs. The broken grey lines indicate a 1 : 1 correspondence.

Figure 8. ^{31}P (14.1 T, 14 kHz MAS) NMR spectra of (a) AlPO STA-2 and (b) Mg-doped STA-2 (Mg : Al : P = 1 : 5 : 6) with the variation in Ω (measured using CSA-amplified PASS experiments as shown in the Supporting Information) across the lineshape indicated by the red points.

Figure 1

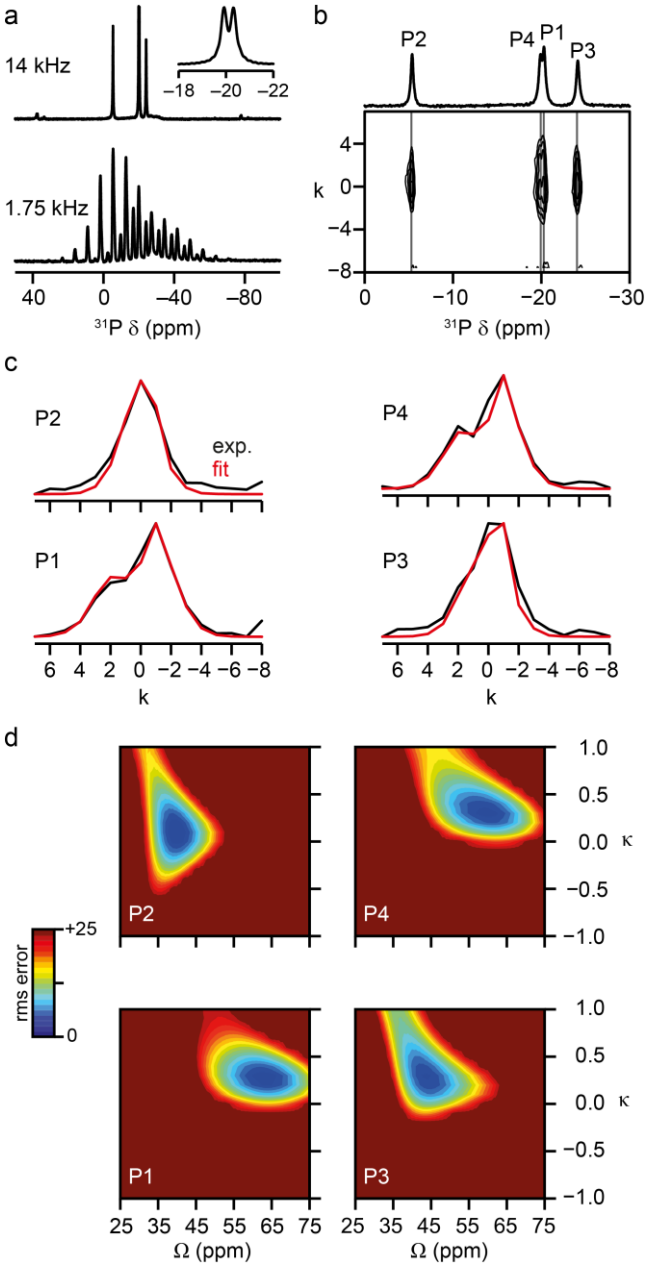
a
14 kHz
−18 −20 −22
1.75 kHz
40 0 −40 −80
31P δ (ppm)
b
P2
P4 P1
P3
4
k 0
−4
−8
0 −10 −20 −30
31P δ (ppm)
c
P2
exp.
fit
P4
P1
P3
6 4 2 0 −2 −4 −6 −8
k
d
P2
P4
P1
P3
+25
rms error
0
1.0
0.5
0.0 κ
−0.5
−1.0
25 35 45 55 65 75
Ω (ppm)

Figure 2

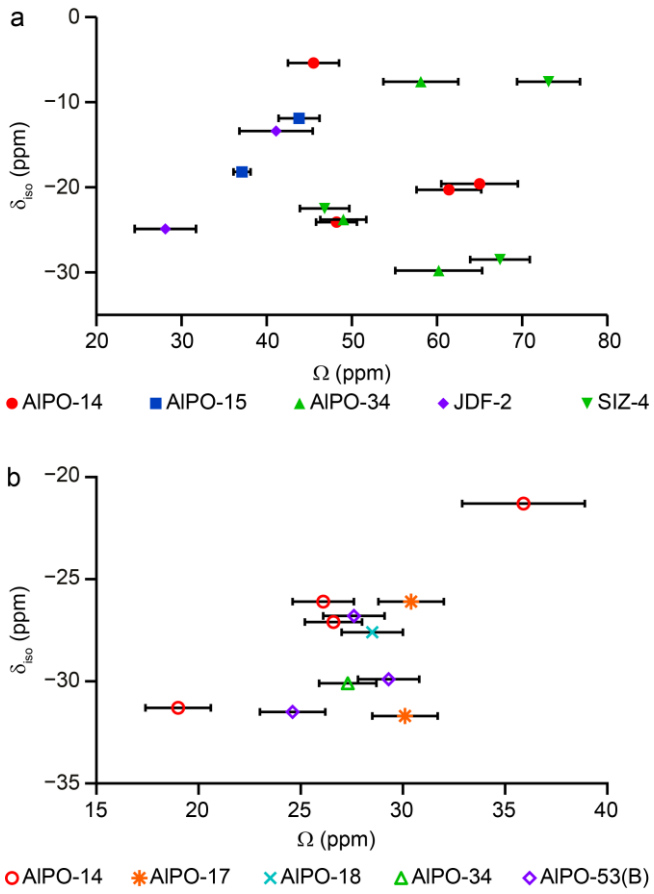
a
0
−10
−20
−30
δiso (ppm)
20
30
40
50
60
70
80
Ω (ppm)
AlPO-14
AlPO-15
AlPO-34
JDF-2
SIZ-4
b
−20
−25
−30
−35
δiso (ppm)
15
20
25
30
35
40
Ω (ppm)
AlPO-14
AlPO-17
AlPO-18
AlPO-34
AlPO-53(B)

Figure 3

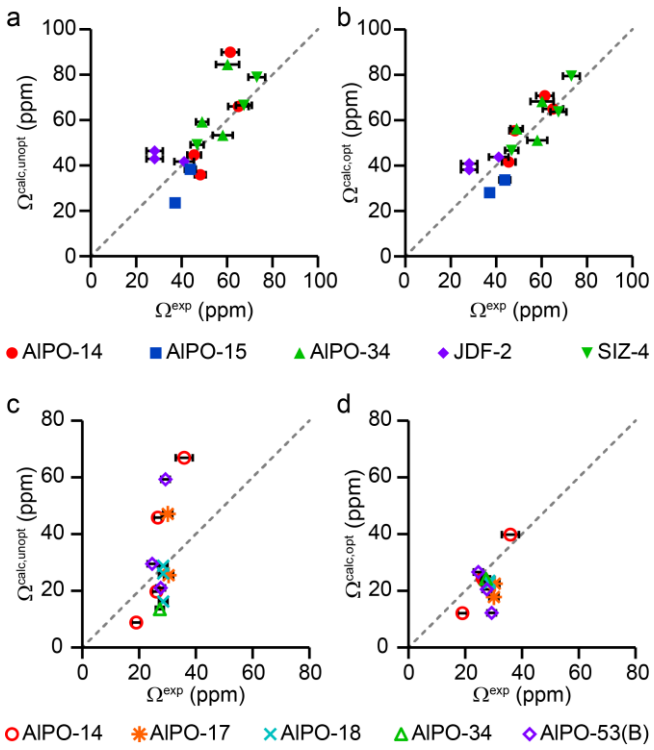
a
b
c
d
Ω^calc.unopt (ppm)
Ω^calc.opt (ppm)
Ω^exp (ppm)
AlPO-14
AlPO-15
AlPO-34
JDF-2
SIZ-4
AlPO-17
AlPO-18
AlPO-53(B)

Figure 4

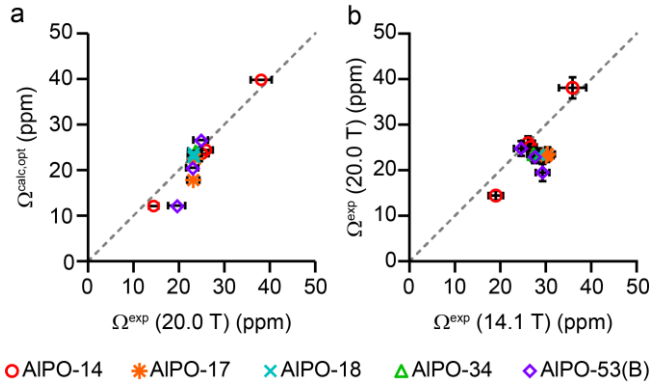

Figure 5

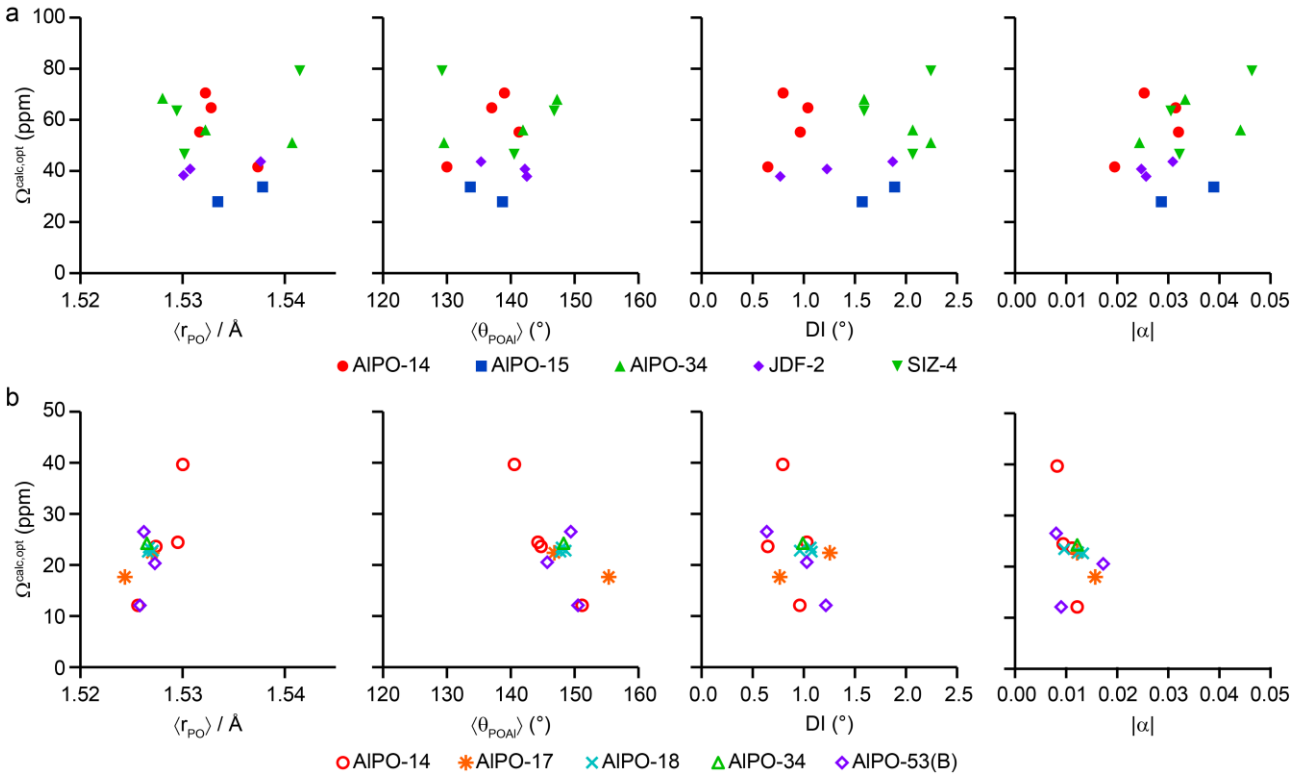

Figure 6

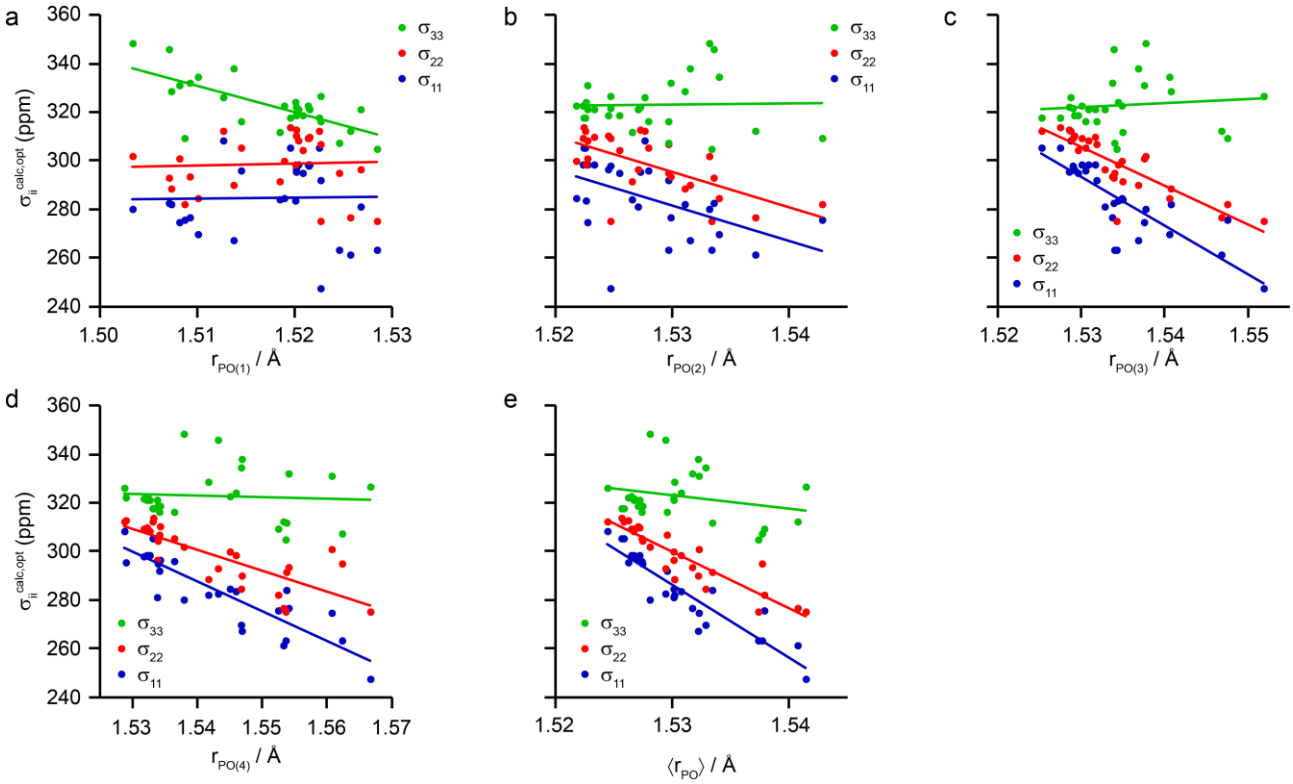
a
b
c
d
e
σ33
σ22
σ11
σii calc,opt (ppm)
rPO(1) / Å
rPO(2) / Å
rPO(3) / Å
rPO(4) / Å
⟨rPO⟩ / Å

Figure 7

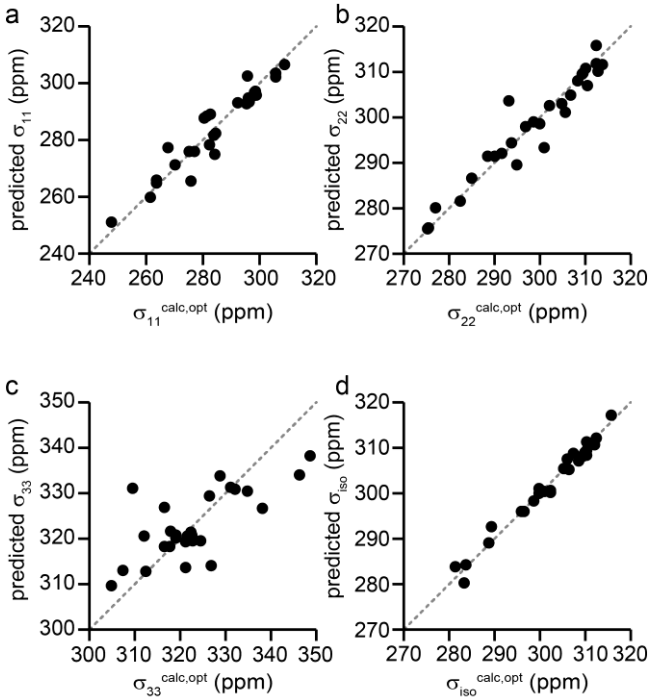

Figure 8

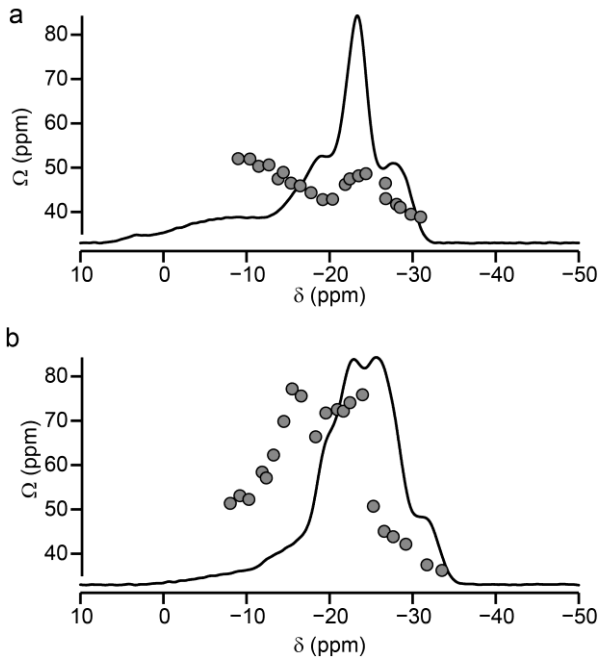

TOC Graphic

Is the ^{31}P Chemical Shift Anisotropy of Aluminophosphates a Useful Parameter for NMR Crystallography?

Daniel M. Dawson*, Robert F. Moran, Scott Sneddon and Sharon E. Ashbrook*

We investigate how to measure the small ^{31}P chemical shift anisotropies (CSAs) of AlPOs, using CSA-amplification experiments and high magnetic field (20.0 T) to obtain an accurate value. For Mg-doped STA-2, the CSA is much larger for $P(OAl)_{4-n}(OMg)_n$ environments, predominantly owing to a much shorter P-O(Mg) bond, which primarily affects δ_{33}. In this case, the CSA information leads to unambiguous assignment of a complicated spectral lineshape.